



Cite this: DOI: 10.1039/c5lc01093d

Using confined bacteria as building blocks to generate fluid flow†

 Zhiyong Gao,^a He Li,^a Xiao Chen^a and H. P. Zhang^{*ab}

In many technological applications, materials are transported by fluid flow at micro/nanometer scales. Conventionally, macroscopic apparatuses, such as syringe pumps, are used to drive the flow. This work explores the possibility of utilizing motile bacteria as microscopic pumps. We used micro-fabricated structures to confine smooth-swimming bacteria in a prescribed configuration. The flagella of confined bacteria rotate to collectively generate flow that can transport materials along designed trajectories. Different structures are combined to realize complex functions, such as collection or dispersion of particles. Experimental findings are reproduced in numerical simulations. Our method opens new ways to generate transport flow at the micrometer scale and to drive bio-hybrid devices.

 Received 13th September 2015,
Accepted 12th October 2015

DOI: 10.1039/c5lc01093d

www.rsc.org/loc

1. Introduction

In a microscopic environment, fluid flow is dominated by viscous effects and the governing Stokes equation has a time-reversal symmetry.^{1–3} This leads to the strange and sometimes counter-intuitive physics of low Reynolds number hydrodynamics. For example, Purcell's "scallop theorem" states that nonreciprocal motion is required for generation of directed flow or motility.⁴ Hence, many familiar macroscopic processes utilizing inertia do not work on small scales and the unique physical constraints of low Reynolds number hydrodynamics have led to several technological challenges, such as efficient transportation of fluid and materials through a microfluidic system.^{5–9}

Microorganisms, such as bacteria, are native inhabitants of the microscopic world. In the evolutionary process, they have acquired swimming strategies which successfully overcome the limitations of viscous effects.^{3,10} For example, a wide variety of bacteria swim by rotating helical filaments, called flagella.^{11,12} Each flagellum is connected to a molecular motor *via* a flexible hook. The motor is anchored in the bacterial cell wall and driven by protons or sodium ions flowing from the outside to the inside of the cell. In peritrichous bacteria, such as *Escherichia coli*, flagella form a bundle that pushes the cell body steadily forward when all motors turn counterclockwise (as seen by an observer on the

outside of the cell looking down at the hook).^{11,13} Bacteria can swim about ten body-length per second with an energy conversion efficiency estimated to be orders of magnitude greater than that of existing synthetic micromotors.⁷

Bacteria have been used to drive bio-hybrid devices.^{8,9} Researchers physically attached bacteria to microscopic cargo and used bacteria as micro-propellers to achieve faster transportation.^{14–19} Free swimming bacteria in suspensions were shown to be able to rotate and translate immersed objects.^{20–23} Researchers also tethered swimmers to a stationary object to generate transport flow. In a pioneering experiment, Darnton *et al.* immobilized motile bacteria on an open surface to form a densely packed monolayer, called a bacterial carpet; the rotating flagella of the tethered bacteria generate a strong flow near the activated surface.¹⁴ In the following studies, bacterial carpets have been used to pump fluid through a microchannel,²⁴ to enhance mixing in microfluidic devices,²⁵ and to investigate collective dynamics of hydrodynamically coupled cells.^{26–28}

These previous studies have clearly demonstrated the possibility of using immobilized bacteria to drive fluid flow.^{14,24,25,27,28} In order to engineer the generated flow, one has to precisely control the position and orientation of immobilized bacteria. Blotting¹⁴ and flow deposition²⁴ methods previously used to create bacterial carpets, however, cannot achieve such a precise control. Here we solve this problem with micro-fabricated structures containing cavities.^{29–31} The cavity size is comparable to that of a bacterial body; each cavity captures a single bacterium with its flagella freely rotating in the fluid. Through careful design of cavities, we can precisely position and orient the bacteria to generate the desired flow pattern. Experimental results are quantitatively reproduced by numerical calculations using

^a Department of Physics and Astronomy and Institute of Natural Sciences, Shanghai Jiao Tong University, Shanghai, China.

E-mail: hepeng_zhang@sjtu.edu.cn

^b Collaborative Innovation Center of Advanced Microstructures, Nanjing, China

† Electronic supplementary information (ESI) available: Fig. S1–S3 and Movies S1–S7. See DOI: 10.1039/c5lc01093d

the regularized Stokeslet method.^{12,32,33} Our work provides a convenient and precise method to control motile bacteria in technological and scientific investigations.

2. Experimental and numerical methods

2.1 Bacteria cultivation

We grew *Escherichia coli* cells (RP5232) overnight in Luria broth (Sigma) in a shaking incubator (37 °C and 200 rpm). The saturated culture was then diluted (1:50) in tryptone broth medium and regrown for 4.5 h at 32 °C and 200 rpm. Cells were then collected from the culture media by centrifugation at 1000g (3680 rpm) for 5 min at room temperature. The resulting pellet was gently re-suspended by mixing in a motility buffer (10^{-2} M glucose, 10^{-4} M EDTA (pH 7.0)).^{20,22} No salts were added to the motility buffer to avoid particle aggregation and adhesion to the coverslip. With the above procedure, we obtained highly motile bacteria with a mean body length of 3 μm (cf. Fig. S1†).

2.2 Micro-fabrication and sample preparation

The structures were fabricated with a two-photon micro-fabrication system (μFAB3D from Teem Photonics). This system uses a microscope objective lens (Zeiss Fluor, 100 \times , numerical aperture 1.3) to focus the pulsed laser (Nd:YAG microchip laser with a 532 nm wavelength, a 750 ps pulse width, and a 40 kHz repetition rate) onto a droplet of the photoresist resin that is mounted on a Piezo nanopositioning Stage (PI P-563.3CL). We used a biocompatible resin ORMOCOMP (Micro resist technology GmbH) with a photo-initiator (1,3,5-tris(2-(9-ethylcabazyl-3)ethylene)benzene). Photopolymerization occurs and solidifies the resin at the focal point, and the Piezo stage scans the resin relative to the focal point in a designed 3-dimensional pattern to fabricate the structures.³⁴ After the scanning was finished, we removed the remaining liquid resin by washing the structure with 4-methyl-2-pentanone and acetone respectively for 5 minutes. Our technique can fabricate structures with a sub-micrometer resolution. Fig. 1(a) shows a scanning electron micrograph (Zeiss Ultra Plus) of the structure fabricated on a cover slip.

To prepare the sample, we immersed the structures in a motility buffer containing the bacteria and flow tracers. Then the sample was enclosed in a sealed chamber and mounted on a Nikon inverted microscope for imaging.

2.3 Imaging and velocity measurement

The motion of the fluorescent flow tracers (0.49 μm in diameter, F8813, Invitrogen) was recorded through a 60 \times oil objective lens (numerical aperture 1.4) at a rate of 40 frames per second with a Basler camera (acA2040-90um). For each experiment, 10 000 images were obtained and analyzed with a custom Matlab software program that precisely tracks the tracers with standard particle tracking algorithms. The resulting

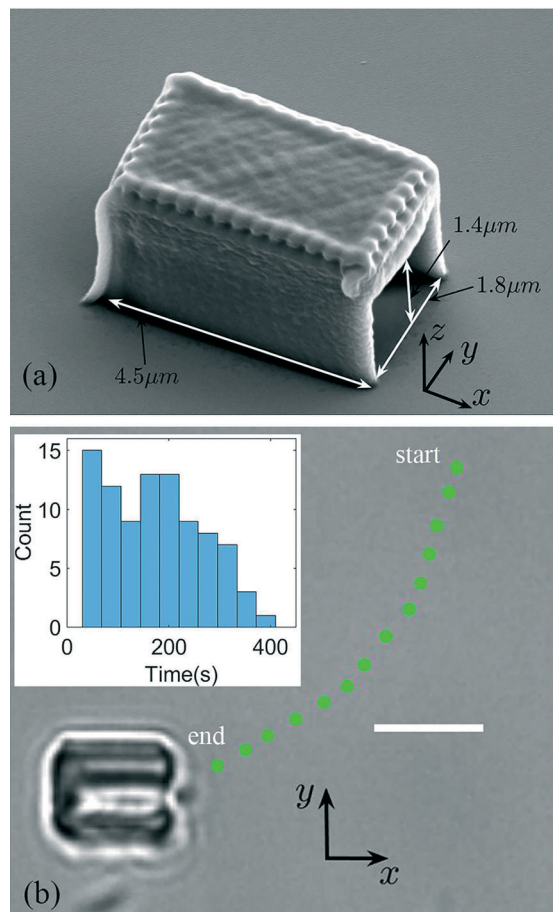


Fig. 1 (a) Scanning electron micrograph of a structure. The thickness of the top and side walls is 1.4 μm and 0.6 μm , respectively. (b) Phase-contrast image of a bacterium confined in a structure (scale bar: 5 μm). The green dots show the bacteria trajectory before being captured. The inset shows the distribution of filling time (see the text) for 90 events.

tracer velocity vectors were spatially binned into a 1 μm square grid and the mean of the vectors in each bin was taken as a measure of the time-averaged local flow.

We used a defocusing method³⁵ to track the 3D trajectories of the fluorescent tracers. When a fluorescent tracer is away from the focal plane of the objective, the tracer's defocused image appears as a bright ring. The ring radius changes with the separation between the tracer and the focal plane. Therefore, we can infer the tracer's 3D position from the size and position of the defocused ring.

2.4 Numerical simulations

To complement the experimental results, we carried out numerical simulations with the regularized Stokeslet method.^{12,32,33} Our model for a single confined bacterium is shown in Fig. 2(d). In the model, a helix rotates behind a vertical wall and above a coverslip. Geometric parameters for the helix are chosen to match those of the *E. coli* flagellum:¹² pitch 2 μm , coil radius 0.25 μm , axial length 4 μm , and

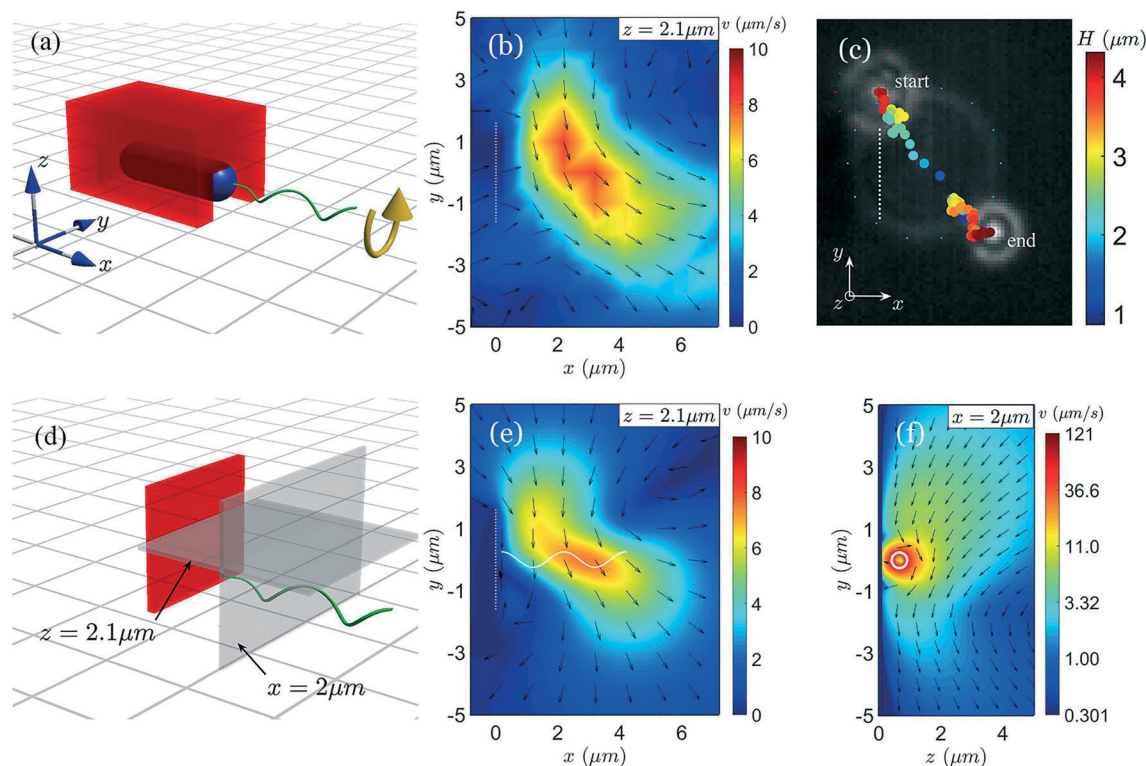


Fig. 2 (a) Illustration of a motile bacterium confined in a structure. The yellow arrow shows the direction of flagellar rotation. (b) Fluid flow measured on the xy plane at $z = 2.1 \mu\text{m}$ above the coverslip in experiments. Movie S2[†] shows two dimensional trajectories of fluorescent tracers. (c) A three dimensional tracer trajectory color-coded by the tracer height above the coverslip. Three defocused rings with their fit are shown in the background. (d) Illustration of the numerical model. The structure and cell body are represented by a no-slip wall (shown in red). (e–f) Flow fields computed on two planes at $z = 2.1 \mu\text{m}$ and $x = 2 \mu\text{m}$. The color in (b), (e), and (f) represents the velocity magnitude and the arrows denote the direction of flow. The white dashed lines in (b–c) and (e) mark the right boundary of the structure and the wall, respectively. The projections of flagella on the measurement plane are shown as white solid lines in (e) and (f).

filament radius $0.012 \mu\text{m}$. The size of the vertical wall is chosen to be that of the yz cross section of the structure. The helix is discretized as a string of 424 Stokeslets; the nearest Stokeslets are separated by $0.012 \mu\text{m}$. The wall is represented by Stokeslets on a square grid with a spacing of $0.1 \mu\text{m}$. Following ref. 36, we used $0.07 \mu\text{m}$ and $0.01 \mu\text{m}$ as the regularization parameters for the Stokeslets on the wall and the helix, respectively. No-slip boundary condition is required on the wall, the helix, and the coverslip. An imaging method³³ is used to realize the boundary condition on the coverslip. We averaged the flow fields over different phases of a rotating period to generate a time-averaged field, which was compared with the experimental results. In simulations of multiple flagella, we assigned random initial phases to the flagella. Other configurations of the initial phases were tested and we found that the time-averaged flow doesn't depend on the initial phases.

3. Results

3.1 Confinement of a motile bacterium

The structures are fabricated on coverslips and contain cubic cavities of $4.5 \times 1.8 \times 1.4 \mu\text{m}^3$ (cf. Fig. 1(a)). When a smooth-swimming *E. coli* bacterium swims into a cavity by chance, it

will be captured because of its inability to swim back-out of the cavity by rotating the flagella bundle in a clockwise direction.³⁰ A typical capture process is shown in Fig. 1(b) and Movie S1[†]. The structure used to produce Fig. 1(b) is intentionally made shorter ($3 \mu\text{m}$), so part of the cell body is outside the structure and body motion can be seen clearly in Movie S1[†] which demonstrates the vitality of the confined bacterium.

We used a dilute bacteria suspension with a volume fraction less than 0.1%. Bacteria accumulate near the coverslip and swim parallel to the boundary:^{37–39} both effects increase the efficiency of filling the structures with bacteria. We measure the time it takes to fill a cavity after the sample is prepared and plot the distribution of filling time for 90 capture events in the insert of Fig. 1(b). Under our experimental conditions, the mean filling time is 3 minutes.

3.2 Fluid flow generated by a confined bacterium

We first investigate the fluid flow around a single confined bacterium. As shown in Fig. 2(a), the cavity has a suitable size so that the body of a typical bacterium is inside and the flagellar bundle (represented by a single flagellum) rotates outside to generate fluid flow. The corresponding numerical

model is shown in Fig. 2(d). To reduce computing costs, we don't explicitly treat the structure and cell body in simulations; their hydrodynamic effects are represented by a vertical wall, which has the same size ($3.0 \times 2.8 \mu\text{m}^2$) as the yz cross section of the structure. The flagellum rotates around its axis with a frequency of $\Omega = 165 \text{ Hz}$ and the axis is $0.65 \mu\text{m}$ above the bottom surface: $h = 0.65 \mu\text{m}$. The same values of Ω and h are used in all simulations.

To understand the complex flow around the confined bacterium, we recall that the rotation of a helical flagellum generates translational fluid flow along the flagellum axis and rotational flow around the axis.^{13,32} In our study, the flagellum is close to a solid surface and the fluid flow is heavily damped near the coverslip (at $z = 0$), as shown by the computed velocity field on the $x = 2 \mu\text{m}$ plane in Fig. 2(f). This

renders the y -velocity component (V_y) negative in most of the region that is not too close to the flagellum.^{37,39} Consequently, a flow tracer released at the upper-left corner in Fig. 2(c) moves in the negative y direction; the tracer is also advected in the x direction by the translational flow of the helix. This diagonal particle trajectory is consistent with the velocity field on the $z = 2.1 \mu\text{m}$ plane, as shown in Fig. 2(b) and (e). The tracer also exhibits a significant motion in the z direction. As shown in Fig. 2(c), the z coordinate of the tracer first decreases then increases as it moves from the upper-left to the bottom-right corner. This is consistent with the flow field in Fig. 2(f).

As shown in Fig. 2, the flow around a confined bacterium is complex in the near field. In the far field, the flow is simpler and can be understood from the perspective of flow

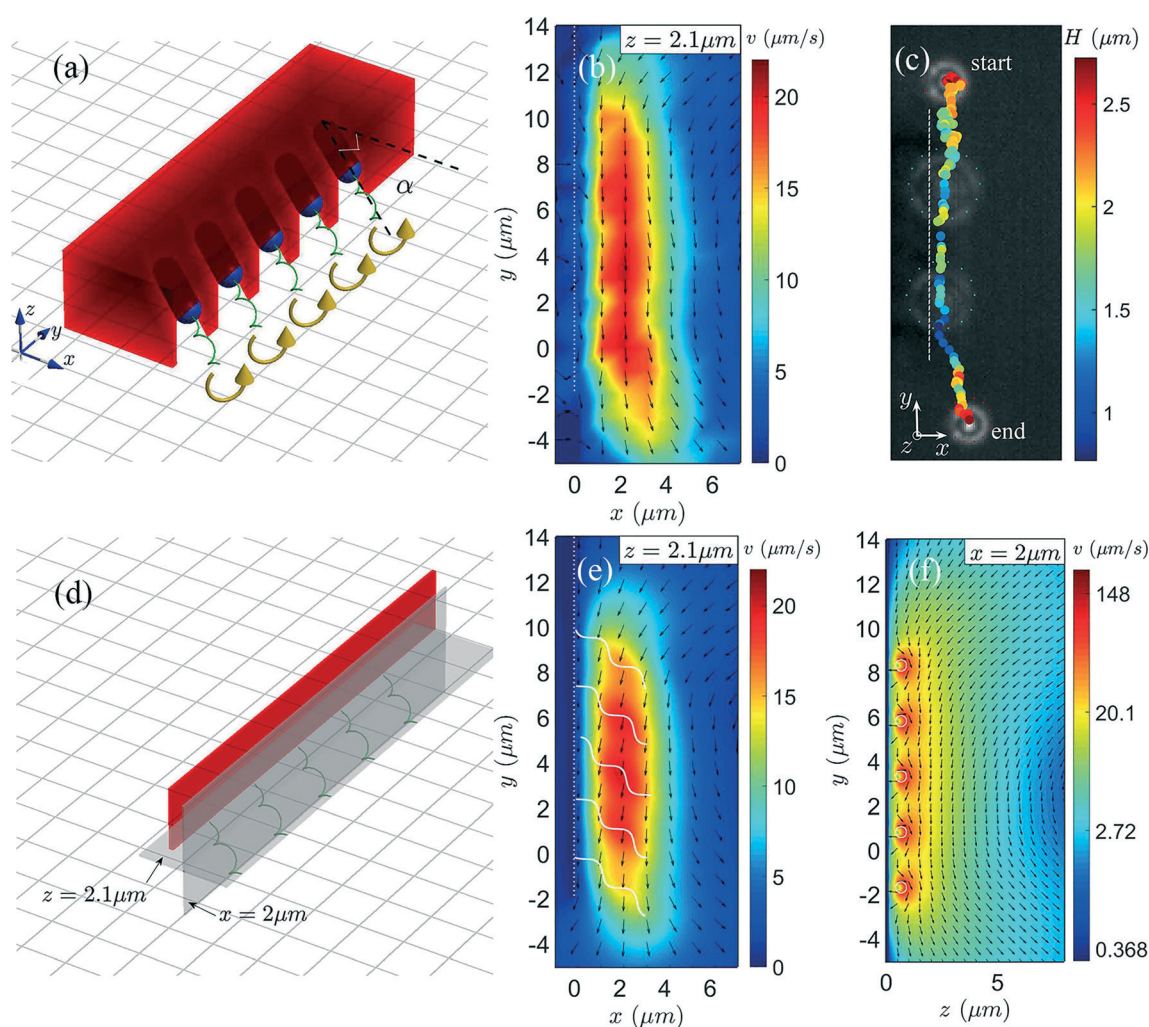


Fig. 3 (a) Illustration of a linear array of 5 confined bacteria. Bacterial flagella tilt at an angle of $\alpha = 40^\circ$. The yellow arrows show the direction of flagellar rotation. An electron micrograph of the structure is shown in Fig. S2.† (b) Fluid flow measured on the xy plane at $z = 2.1 \mu\text{m}$ above the coverslip in experiments. Raw data of tracer motion can be found in Movie S3.† (c) A three dimensional tracer trajectory color-coded by the tracer height above the coverslip. Four defocused rings with their fit are shown in the background. (d) Illustration of the numerical model. The structure and cell bodies are represented by a no-slip wall (shown in red). (e–f) Flow fields computed on two planes at $z = 2.1 \mu\text{m}$ and $x = 2 \mu\text{m}$, respectively. The color in (b), (e), and (f) represents the velocity magnitude and the arrows denote the direction of flow. The white dashed lines in (b–c) and (e) mark the right boundary of the structure and the wall, respectively. The projections of flagella on the measurement plane are shown as white solid lines in (e) and (f).

singularities. A rotating flagellum can be represented by a Stokeslet and a rotlet.^{2,13} In free space, the flow generated by these two singularities has different asymptotic behaviors: $V_{\text{Stokeslet}} \propto 1/r$ and $V_{\text{rotlet}} \propto 1/r^2$, where r is the distance from the singularities, and the far-field flow of a rotating flagellum in free space is dominated by the Stokeslet contribution.^{13,40} However, when the flow singularities are near a no-slip boundary, their hydrodynamic images also contribute to the flow. Blake and Chwang found that, close to a no-slip boundary, two singularities generate flow similarly decaying as $V \propto 1/r^2$ in the far field (except in a few special orientations),⁴¹ therefore their contributions are equally important.

3.3 Fluid flow generated by a linear array of confined bacteria

Fig. 2 clearly demonstrates that a single confined bacterium generates transport flow. We can use confined bacteria as basic building blocks to generate designed flow patterns. For example, Fig. 3(a) shows a linear structure that positions five bacteria along the y direction and orients them by a tilt angle $\alpha = 40^\circ$. As seen in experiments (Fig. 3(b)) and simulations (Fig. 3(e)), the rotating flagella collectively generate a “fluid conveyor”, which has a peak speed of about $20 \mu\text{m s}^{-1}$ and a width of about $5 \mu\text{m}$ in the x -direction. Such a “fluid conveyor” can be qualitatively understood as the superposition of the “L” shaped flow pattern of a single bacterium (*cf.* Fig. 2(b)). The tracer trajectory in Fig. 3(c) supports the picture of a “fluid conveyor”. As we move away from the coverslip, the flow decays from $20 \mu\text{m s}^{-1}$ to a few $\mu\text{m s}^{-1}$ at a height of $z = 5 \mu\text{m}$, as shown in Fig. 3(f).

The transport efficiency of the “fluid conveyor” crucially depends on the tilt angle α . To quantify this effect, we fabricate structures that are similar to the one in Fig. 3(a) but with different tilt angles. The fluid flow on the xy plane at $z = 2.1 \mu\text{m}$ is measured for each structure. We find that the flow pattern remains qualitatively the same (*cf.* Fig. 3(b)) but the flow strength and spatial extent change with α . Quantitatively, we measure the profile of the y -velocity component, $V_y(x)$, in the

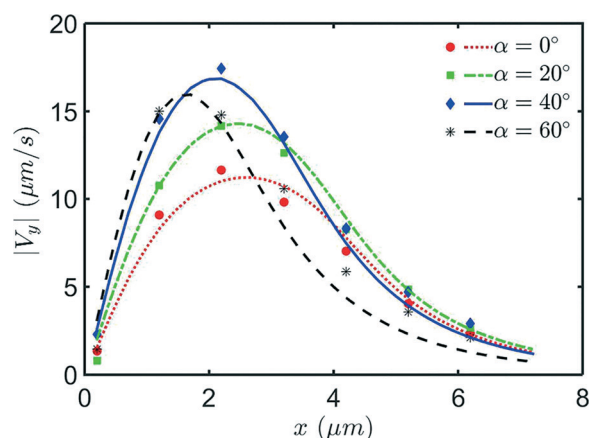


Fig. 4 Profiles of flow strength, $|V_y(x)|$, measured near four structures with different tilt angles, α . Experimental and numerical results are shown by symbols and lines, respectively.

middle region of the structure, where flow doesn't depend strongly on the y -coordinate. The experimental results are shown in Fig. 4 as symbols for four α values. The peak speed is the highest for $\alpha = 40^\circ$. The spatial extent of the flow approximately remains the same for $\alpha \leq 40^\circ$ and becomes smaller for $\alpha = 60^\circ$. Therefore, among the investigated angles, $\alpha = 40^\circ$ gives the highest transport efficiency. This tilt angle will be used in designing the structures in Fig. 5–7. The flow

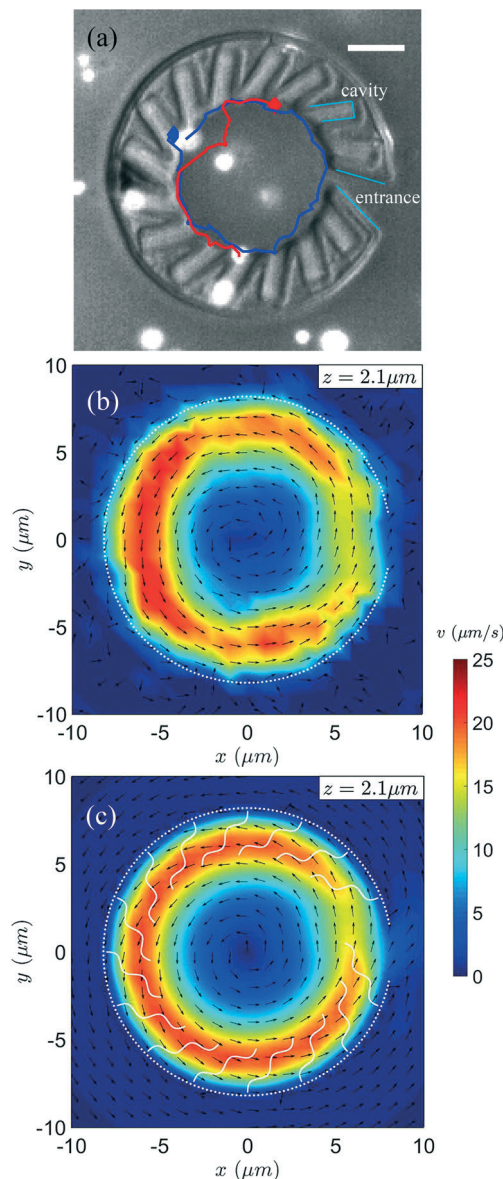


Fig. 5 (a) Optical micrograph of a circular structure and tracer trajectories shown by solid lines. The starting positions of the tracers are marked by symbols. More tracer trajectories can be found in Movie S4.† Scale bar: $5 \mu\text{m}$. Fluid flow measured on the xy plane at $z = 2.1 \mu\text{m}$ in the experiment (b) and in simulation (c). The color in (b) and (c) represents the velocity magnitude and the arrows denote the direction of flow. The white dashed lines in (b) and (c) mark the inner boundary of the structure and the circular wall, respectively. The projections of flagella on the measurement plane are shown as white solid lines in (c). Illustrations of experimental and numerical models are shown in Fig. S3.†

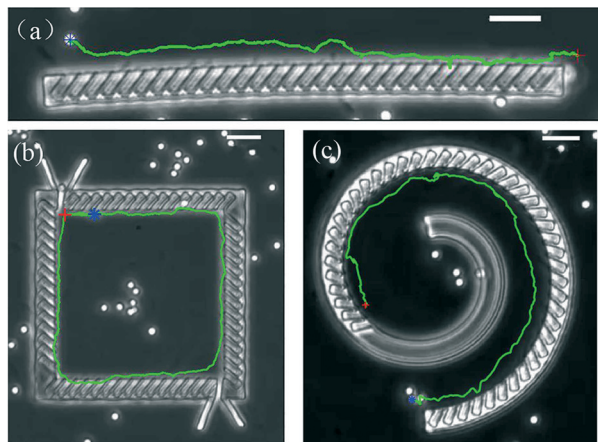


Fig. 6 Transport of silica particles (2 μm in diameter) by bacteria confined in a linear (a), square (b), and spiral (c) structure. The starting and final positions of the tracers are marked by blue and red symbols, respectively. The capturing cavities are tilted with an angle $\alpha = 40^\circ$ with respect to the local tangent of the structures. Scale bar: 10 μm .

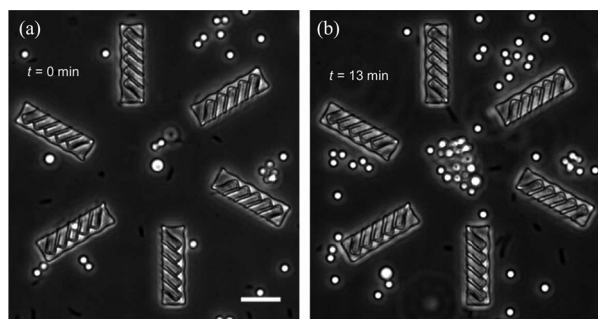


Fig. 7 Targeted transport of silica particles by bacteria confined in 6 linear structures. Initially dispersed particles (a) are transported to the center region after 13 minutes (b). Scale bar: 10 μm .

profiles obtained from simulations agree with the experimental values in Fig. 4. This shows that our numerical model is trustworthy and that the bacterial flagella bundle can be well represented by a single flagellum in our study.

3.4 Fluid flow generated by a circular array of confined bacteria

Confined bacteria can be used to generate transport flow with a complex topology. We arrange 15 cavities around a circle and orient the cavities with a tilt angle $\alpha = 40^\circ$, with respect to the local tangent of the circle, as shown in Fig. 5(a) and S3.† After the bacteria fill all cavities, they generate fluid flow in a counter-clockwise direction, as shown by the tracer trajectories in Fig. 5(a) and Movie S4.† The tracers stay in the focal plane for an extended time; this means that the velocity component in the z direction is small. Quantitative experimental and numerical results are shown in Fig. 5(b) and (c), respectively. The flow component parallel to the structure dominates and is responsible for the generation of the circular particle trajectories in Fig. 5(a). The flow strength and

spatial extent are similar to those in the linear case (cf. Fig. 3). The flow is weaker near the entrance at the 3 o'clock position. The maximal flow speed shown in Fig. 3–5 is about $25 \mu\text{m s}^{-1}$; this limitation is imposed by the swimming capability of *E. coli* bacteria. It should be possible to generate faster flow by using microorganisms with higher swimming speeds.¹⁰

3.5 Transport of colloidal particles along designed trajectories

Fig. 4 and 5 show that confined bacteria can generate directed flow along both linear and curved structures. We test the robustness of this phenomenon with more structures and use this phenomenon to transport materials along designed trajectories. As shown in Fig. 6(a) (Movie S5†), thirty bacteria are confined in a linear structure and they collectively generate flow that transports silica particles (2 μm in diameter) over 60 μm in 15 seconds. Particle transportation along a square and a spiral structure is shown in Fig. 6(b) (Movie S6†) and (c) (Movie S7†), respectively.

Our structure-based approach is modular; we can combine different structures to realize complex functions. For example, confined bacteria can be used to collect particles to a defined location.²² In Fig. 7, we position bacteria to generate flow pointing to a focal point and the flow quickly collects the particles to the focus. If we reverse the flow by changing the cell orientation, we can efficiently disperse materials from a location.

4. Discussion

In our approach, each smooth-swimming bacterium is confined in a cavity. This confinement is not permanent but reversible. If a confined bacterium loses motility, it will leave the cavity through thermal diffusion and a new motile bacterium can refill the cavity. This would significantly extend the operating lifetime and stability of the device. For example, our longest test lasts for four hours and the transport flow remains stable throughout the experiment. In contrast, previous works^{42,43} permanently attach bacteria to surfaces, therefore, a non-functioning bacterium cannot be replaced and will leave a permanent defect in the generated flow pattern. This harms the performance and longevity of the device. Optical tweezers can control bacteria with excellent precision and flexibility.^{44–46} However, tweezers can only handle a limited number of cells and it is also hard to completely avoid photo-damage to bacteria.

Many experiments have been performed on either a single bacterium^{12,44,46} or on a collection of many bacteria.^{47–49} Between these two limits, controlled experimental studies of a few bacteria are rare.⁵⁰ Our method can confine multiple bacteria in close proximity and open the door to study the hydrodynamic interactions between their rotating flagella.^{13,46,51} Such experiments may shed light on important issues, such as hydrodynamic synchronization and formation of bacterial flagella bundles.

In summary, we have used cavities of bacterial size to confine smooth-swimming bacteria in prescribed configurations. The rotating flagella of confined bacteria collectively generate transport flow on the micrometer scale. The generated flow can be controlled by changing the location and orientation of the cavities. Experimental results are reproduced by numerical simulations, demonstrating the reliability of our numerical method. We believe that our approach will be useful both for generating new bio-hybrid devices and for studying fundamental interactions between multiple bacteria.

Acknowledgements

We acknowledge financial support from the NSFC (No. 11422427), the Program for Professor of Special Appointment at Shanghai Institutions of Higher Learning (No. SHDP201301), and the Innovation Program of Shanghai Municipal Education Commission (No. 14ZZ030).

References

- 1 C. Brennen and H. Winet, *Annu. Rev. Fluid Mech.*, 1977, **9**, 339–398.
- 2 S. Kim and J. S. Karilla, *Microhydrodynamics: Principles and Selected Applications*, Butterworth-Heinemann, Boston, MA, 1991.
- 3 E. Lauga and T. R. Powers, *Rep. Prog. Phys.*, 2009, **72**, 096601.
- 4 E. M. Purcell, *Am. J. Phys.*, 1977, **45**, 3–11.
- 5 T. M. Squires and S. R. Quake, *Rev. Mod. Phys.*, 2005, **77**, 977–1026.
- 6 G. M. Whitesides, *Nature*, 2006, **442**, 368–373.
- 7 W. Wang, W. Duan, S. Ahmed, T. E. Mallouk and A. Sen, *Nano Today*, 2013, **8**, 531–554.
- 8 R. W. Carlsen and M. Sitti, *Small*, 2014, **10**, 3831–3851.
- 9 V. Chan, H. H. Asada and R. Bashir, *Lab Chip*, 2014, **14**, 653–670.
- 10 J. S. Guasto, R. Rusconi and R. Stocker, *Annu. Rev. Fluid Mech.*, 2012, **44**, 373–400.
- 11 H. C. Berg, *Phys. Today*, 2000, **53**, 24–29.
- 12 B. Rodenborn, C. H. Chen, H. L. Swinney, B. Liu and H. P. Zhang, *Proc. Natl. Acad. Sci. U. S. A.*, 2013, **110**, E338–E347.
- 13 N. Watari and R. G. Larson, *Biophys. J.*, 2010, **98**, 12–17.
- 14 N. Darnton, L. Turner, K. Breuer and H. C. Berg, *Biophys. J.*, 2004, **86**, 1863–1870.
- 15 S. Martel, C. C. Tremblay, S. Ngakeng and G. Langlois, *Appl. Phys. Lett.*, 2006, **89**, 233904.
- 16 B. Behkam and M. Sitti, *Appl. Phys. Lett.*, 2007, **90**, 023902.
- 17 E. Steager, C. B. Kim, J. Patel, S. Bith, C. Naik, L. Reber and M. J. Kim, *Appl. Phys. Lett.*, 2007, **90**, 263901.
- 18 S. J. Park, H. Bae, J. Kim, B. Lim, J. Park and S. Park, *Lab Chip*, 2010, **10**, 1706–1711.
- 19 R. W. Carlsen, M. R. Edwards, J. Zhuang, C. Pacoret and M. Sitti, *Lab Chip*, 2014, **14**, 3850–3859.
- 20 R. Di Leonardo, L. Angelani, D. Dell'Arciprete, G. Ruocco, V. Iebba, S. Schippa, M. P. Conte, F. Mecarini, F. De Angelis and E. Di Fabrizio, *Proc. Natl. Acad. Sci. U. S. A.*, 2010, **107**, 9541–9545.
- 21 A. Sokolov, M. M. Apodaca, B. A. Grzybowski and I. S. Aranson, *Proc. Natl. Acad. Sci. U. S. A.*, 2010, **107**, 969–974.
- 22 N. Koumakis, A. Lepore, C. Maggi and R. Di Leonardo, *Nat. Commun.*, 2013, **4**, 2588.
- 23 A. Kaiser, A. Peshkov, A. Sokolov, B. ten Hagen, H. Lowen and I. S. Aranson, *Phys. Rev. Lett.*, 2014, **112**, 158101.
- 24 M. J. Kim and K. S. Breuer, *Small*, 2008, **4**, 111–118.
- 25 M. J. Kim and K. S. Breuer, *Phys. Fluids*, 2004, **16**, L78–L81.
- 26 N. Uchida and R. Golestanian, *Phys. Rev. Lett.*, 2010, **104**, 178103.
- 27 Y. T. Hsiao, J. H. Wang, Y. C. Hsu, C. C. Chiu, C. J. Lo, C. W. Tsao and W. Y. Woon, *Appl. Phys. Lett.*, 2012, **100**, 203702.
- 28 Y. T. Hsiao, J. H. Wang, K. T. Wu, J. J. Tsai, C. H. Chang and W. Y. Woon, *Appl. Phys. Lett.*, 2014, **105**, 203702.
- 29 D. B. Weibel, W. R. DiLuzio and G. M. Whitesides, *Nat. Rev. Microbiol.*, 2007, **5**, 209–218.
- 30 B. Kaehr and J. B. Shear, *Lab Chip*, 2009, **9**, 2632–2637.
- 31 F. J. H. Hol and C. Dekker, *Science*, 2014, **346**, 438–438.
- 32 R. Cortez, L. Fauci and A. Medovikov, *Phys. Fluids*, 2005, **17**, 031504.
- 33 J. Ainley, S. Durkin, R. Embid, P. Boindala and R. Cortez, *J. Comput. Phys.*, 2008, **227**, 4600–4616.
- 34 M. Malinauskas, M. Farsari, A. Piskarskas and S. Juodkazis, *Phys. Rep.*, 2013, **533**, 1–31.
- 35 M. Wu, J. W. Roberts and M. Buckley, *Exp. Fluids*, 2005, **38**, 461–465.
- 36 Y. Hyon, Marcos, T. R. Powers, R. Stocker and H. C. Fu, *J. Fluid Mech.*, 2012, **705**, 58–76.
- 37 E. Lauga, W. R. DiLuzio, G. M. Whitesides and H. A. Stone, *Biophys. J.*, 2006, **90**, 400–412.
- 38 A. P. Berke, L. Turner, H. C. Berg and E. Lauga, *Phys. Rev. Lett.*, 2008, **101**, 038102.
- 39 S. E. Spagnolie and E. Lauga, *J. Fluid Mech.*, 2012, **700**, 105–147.
- 40 K. Drescher, J. Dunkel, L. H. Cisneros, S. Ganguly and R. E. Goldstein, *Proc. Natl. Acad. Sci. U. S. A.*, 2011, **108**, 10940–10945.
- 41 J. Blake and A. Chwang, *J. Eng. Math.*, 1974, **8**, 23–29.
- 42 J. Kim, Y.-H. Shin, S.-H. Yun, D.-S. Choi, J.-H. Nam, S. R. Kim, S.-K. Moon, B. H. Chung, J.-H. Lee, J.-H. Kim, K.-Y. Kim, K.-M. Kim and J.-H. Lim, *J. Am. Chem. Soc.*, 2012, **134**, 16500–16503.
- 43 M. Woerdemann, F. Horner and C. Denz, *Optofluidics, Microfluidics and Nanofluidics*, 2014, **2014**, 1.
- 44 S. Chattopadhyay, R. Moldovan, C. Yeung and X. L. Wu, *Proc. Natl. Acad. Sci. U. S. A.*, 2006, **103**, 13712–13717.
- 45 U. Mirsaidov, W. Timp, K. Timp, M. Mir, P. Matsudaira and G. Timp, *Phys. Rev. E: Stat., Nonlinear, Soft Matter Phys.*, 2008, **78**, 021910.
- 46 P. J. Mears, S. Koirala, C. V. Rao, I. Golding and Y. R. Chemla, *Elife*, 2014, **3**, e01916.
- 47 A. Sokolov, I. S. Aranson, J. O. Kessler and R. E. Goldstein, *Phys. Rev. Lett.*, 2007, **98**, 158102.

- 48 X. Chen, X. Dong, A. Be'er, H. L. Swinney and H. Zhang, *Phys. Rev. Lett.*, 2012, **108**, 148101.
- 49 E. Lushi, H. Wioland and R. E. Goldstein, *Proc. Natl. Acad. Sci. U. S. A.*, 2014, **111**, 9733–9738.
- 50 D. R. Brumley, K. Y. Wan, M. Polin and R. E. Goldstein, *Elife*, 2014, **3**, e02750.
- 51 M. Kim, J. C. Bird, A. J. Van Parys, K. S. Breuer and T. R. Powers, *Proc. Natl. Acad. Sci. U. S. A.*, 2003, **100**, 15481–15485.